Autonomous Orbit Coordination for Two Unmanned Aerial Vehicles

Rolf Rysdyk*, Christopher Lum†
and Juris Vagners‡
Autonomous Flight Systems Laboratory
University of Washington, Seattle, WA 98195

ABSTRACT

This work considers autonomous coordination between two Unmanned Aerial Vehicles in orbit about a target, with the purpose of geo-locating the target. Wind significantly affects the relative phase angle between the vehicles. Guidance algorithms are investigated to maintain an approximately constant phase angle in wind. A planar-kinematic aircraft model is proposed in which the effects of attitude dynamics and nonlinearities are considered.

1. NOMENCLATURE

χ	Course, [rad]
V_a	Airspeed, [m/s]
V_g	Inertial speed, [m/s]
V_o	Nominal inertial speed, [m/s]
V_w	Windspeed, [m/s]
ψ_p	Clock angle, or bearing from orbit center, [rad]
ψ	Heading, [rad]
ψ_w	Wind direction (from), [rad]
$\vec{V}$	Velocity, [m/s]
x_N	North position [m]
y_E	East position [m]
R	Radius of orbit, [m]

Subscripts

w	Wind
e	Earth fixed North-East-Down frame (NED)
b	Body fixed frame
$1, 2$	Vehicle $1, 2$

2. INTRODUCTION

Two UAVs are to coordinate their observation of a target autonomously. The target location is only roughly known. It is presumed that some on-board sensing is in place to establish the relative target position. The UAVs are commanded to orbit about the estimated position of the target. The goal of the observation is to geo-locate the target, i.e. to accurately determine the absolute target location.[1] A stand-off procedure is preferred to direct over-flight to reduce the chances of detection. A stand-off geo-location process can be optimized by orienting the sensor ranges perpendicularly.[1] Therefore, it is desirable for the UAVs to maintain approximately 90^o angular-phase relative to each other, figure 1. The UAVs initially coordinate their sensor imagery of the target by being co-located on the orbit, after which separation should occur to improve the geo-location of the target. In this work we investigate some feedback structures to achieve tracking of desired relative phase angles. Considerations include the effects of significant wind, and the fact that direct manipulation of airspeed is limited.

The current work is demonstrated in hardware-in-the-loop simulation of flight with two ScanEagle aircraft.[2] The geometry of a typical stand-off observation orbit for these aircraft is designed as:

*Assistant Professor, Department of Aeronautics and Astronautics, email: rysdyk@aa.washington.edu
†Graduate Student, Department of Aeronautics and Astronautics, email: lum@u.washington.edu
‡Professor Emeritus, Department of Aeronautics and Astronautics, email: vagners@aa.washington.edu

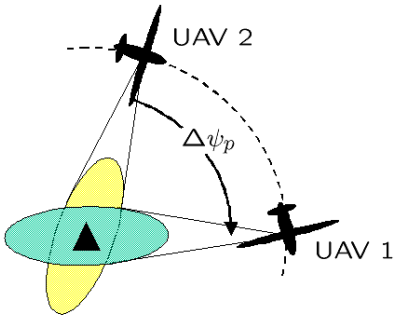

Fig. 1 Geo-locating a target with two vehicles.

- The nominal radius $R_o = 200[m]$.
- Altitude of the vehicles, $h_1 = 1000[ft]$ and $h_2 = 1100[ft]$.
- Airspeed manipulation assumed at $\approx 20 < V_a < 35[m/s]$ with first order dynamics.
- Radius manipulation assumed as $0.9R_o < R_2 < 1.1R_o$, where R_o is the nominal radius, and R_2 refers to vehicle 2.

3. THE EFFECT OF WIND

Wind is expected to be a major factor in the guidance of a flock of small UAVs. It is of interest to see what the effect of wind is on the relative phase angle between vehicles in orbit. We investigate the following examples:

1. Given that both vehicles maintain constant airspeed of $25\ m/s$, and given a relative phase angle of 90^o at some point on orbit, how does the relative phase angle vary around the orbit? (Figure 4.)
2. Given that vehicle 1 maintains a constant airspeed in orbit, what is the required change in airspeed of vehicle 2 to maintain a 90^o relative phase angle? (Figure 5.)
3. If both vehicles can adjust airspeed, what variation is required to maintain 90^o phasing? (Figure 6.)
4. Given that manipulation of airspeed may be limited, can the orbit radius of one of the vehicles be altered to control the relative phase angle? (Figures 10-18.)

Using vector notation to include wind and express its relation to ground velocity, figure 2, provides:

$$\vec{V}_a + \vec{V}_w = \vec{V}_g \tag{1}$$

Expressed along the NED-frame, this is

$$\begin{pmatrix} V_a \cos\psi \\ V_a \sin\psi \\ 0 \end{pmatrix}_e + \begin{pmatrix} -V_w \cos\psi_w \\ -V_w \sin\psi_w \\ 0 \end{pmatrix}_e = \begin{pmatrix} V_g \cos\chi \\ V_g \sin\chi \\ 0 \end{pmatrix}_e$$

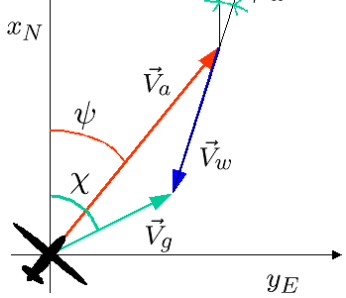

Fig. 2 The effect of wind; definitions for heading ψ, course χ, and wind direction ψ_w.

where ψ is referred to as 'heading', and χ as 'course'. The wind direction is ψ_w, which is defined relative to the NED-frame as the compass direction from which the airmass is coming.
From the NED-components we obtain two expressions:

$$V_a \cos(\psi) = V_g \cos(\chi) + V_w \cos(\psi_w) \quad (2)$$
$$V_a \sin(\psi) = V_g \sin(\chi) + V_w \sin(\psi_w) \quad (3)$$

These expressions apply independently to both vehicles, which are indicated in what follows with subscripts $1, 2$. Of the variables, we assume that the airspeed of vehicle 1 is constant at $V_{a1} = 25m/s$. Wind-speed and direction are assumed known[3] and for convenience of analysis we select $\psi_w = 0$. Since we are not concerned with the heading of either vehicle, these can be eliminated from the expressions, to obtain:

$$V_a^2 = V_g^2 + V_w^2 + 2V_g V_w \cos(\chi) \quad (4)$$

The groundspeed of vehicle 1 can then be expressed as:

$$V_{g1} = -V_w \cos(\chi_1) + V_{a1}\sqrt{1 - \left(\frac{V_w}{V_{a1}}\right)^2 \sin^2(\chi_1)} \quad (5)$$

Consider figure 3, while the vehicle remains on orbit, the following holds.

$$\chi_1 = \psi_{p1} + \pi/2 \quad (6)$$
$$\dot{\psi}_{p1} = V_{g1}/R \quad (7)$$

Combining the results applied for both vehicles gives:

$$\Delta\dot{\psi}_p \triangleq \dot{\psi}_{p1} - \dot{\psi}_{p2} = (V_{g1} - V_{g2})/R \quad (8)$$

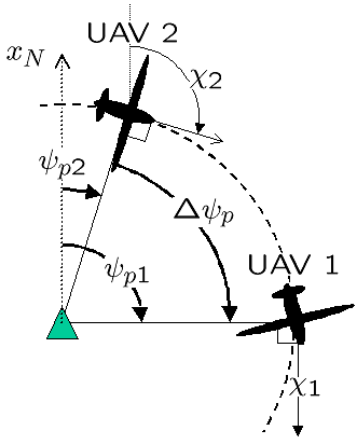

Fig. 3 Definition of relative phase angle between two vehicles.

recreated from Eqns(5) and (6) applied to both vehicles, and

$$\Delta\dot{\psi}_p = (V_{g1} - V_{g2})/R$$
$$\dot{\psi}_{p1} = V_{g1}/R$$
$$\psi_{p2} = \psi_{p1} - \Delta\psi_p$$

The results are displayed in figure 4. These results indicate that for mild wind conditions the phasing may remain satisfactory for purposes of geo-locating. However, for high wind conditions or to optimize the geo-locating, some regulation of relative phase angle is desirable.

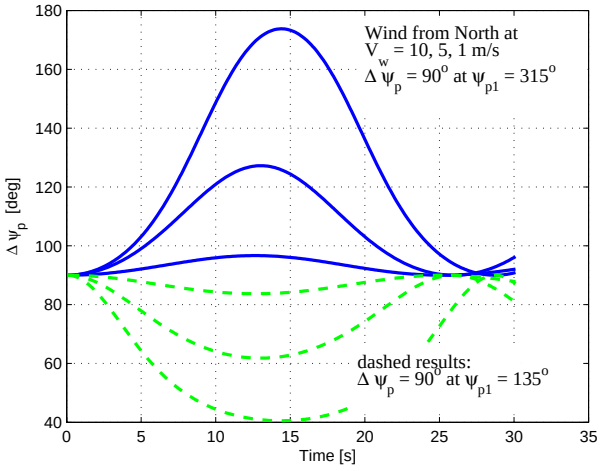

Fig. 4 Effect of wind on the relative phase angle with both vehicles operating at constant airspeed. The maximum and minimum depend on where the vehicles are phased at 90^o. The results give approximately the worst case situations.

If, rather than maintaining V_{a2} constant, we manipulate it to maintain the relative phase angle $\Delta\psi_p = 90^o$, then

$$V_{g2} = V_{g1}$$
$$\psi_{p2} = \psi_{p1} - \pi/2$$

this also implies $\chi_2 = \psi_{p1}$. From the foregoing we can obtain an expression for the required airspeed of vehicle 2 in terms of the clock-angle of vehicle 1:

$$V_{a2} = \sqrt{V_{g1}^2 + V_w^2 + 2V_{g1}V_w \cos(\psi_{p1})} \quad (9)$$

The result is indicated in figure 5. A windspeed of $10m/s$ would require airspeed manipulation of up to almost three times that amount.

If both vehicles adjust their airspeed to maintain a constant relative phase angle, the required changes in airspeed are dramatically lower. This is shown in figure 6.

4. A PLANAR-KINEMATIC AIRCRAFT MODEL

For design and analysis of the orbiting guidance algorithms we will reduce the aircraft dynamic model to a planar-kinematic model, figure 7. We will be concerned with the inertial position of the aircraft, which we express in terms of the inertial course and ground speed:

$$\dot{x}_N = V_g \cos\chi \quad (10)$$
$$\dot{y}_E = V_g \sin\chi \quad (11)$$

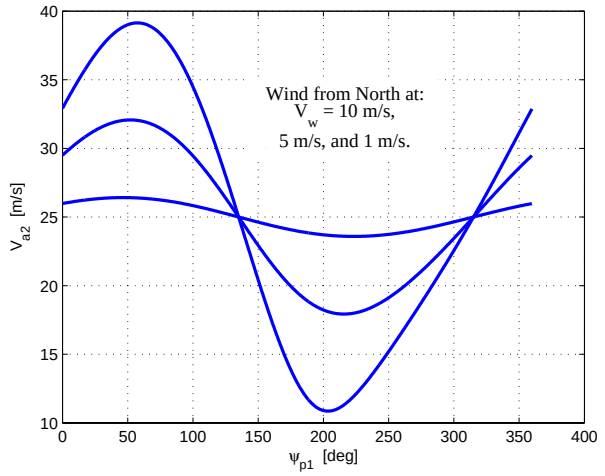

Fig. 5 Required changes in airspeed of vehicle 2 to maintain a constant 90^o phasing between vehicles, while vehicle 1 maintains $V_{a1} = 25\ m/s$.

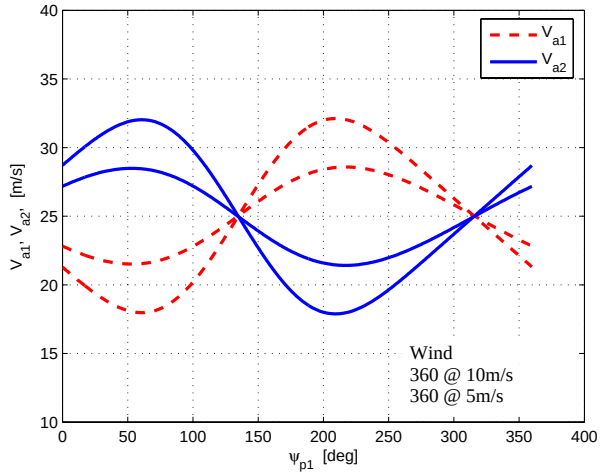

Fig. 6 Required changes in airspeed to maintain a constant relative phase angle of 90^o, while both vehicles maintain an average airspeed of $25\ m/s$.

The effect of wind is included as Eqns 2, repeated here for completeness of model formulation.

$$V_a \cos(\psi) = V_g \cos(\chi) + V_w \cos(\psi_w) \quad (12)$$
$$V_a \sin(\psi) = V_g \sin(\chi) + V_w \sin(\psi_w) \quad (13)$$

The aircraft is assumed to operate with coordinated turns, i.e. with the resultant acceleration in the aircraft-plane of symmetry. The planar kinematic approximation of a coordinated turn links the bank angle to the course-rate of change as:

$$\dot{\chi} = \frac{g}{V_g} \tan\phi \quad (14)$$

Wind also affects the relation between course and heading. The heading is obtained from the above navigation equations as:

$$\psi = \text{atan2}\left\{ \frac{V_g \sin\chi + V_w \sin\psi_w}{V_g \cos\chi + V_w \cos\psi_w} \right\} \quad (15)$$

where atan2 represents the 4-quadrant tangent function.

Time scale separation between navigation and bank-angle dynamics allow the bank-angle to be considered as a control signal for navigation purposes. The aircraft under consideration in this work shows bank angle dynamics to be approximately first order as:

$$\tau_\phi \dot{\phi} = -\phi + \phi_c \quad (16)$$

angle, and the time constant $\tau_\phi \approx 1/2.7\ s$. Furthermore, ϕ_c is limited to $\pm 45^o$ and rate-limited to $\pm 45^o/s$. The remaining control degree of freedom considered in this work is the airspeed. The dynamics associated with airspeed manipulation depend on engine dynamics, atmospheric conditions, and propeller efficiency. We approximate the airspeed response as a rate limited first order system with hard bounds on the output, where $\tau_V = 1\ s$.

$$\tau_V \dot{V}_a = -V_a + V_{ac} \quad (17)$$

Eqns(10) through (17) describe aircraft motion at constant altitude, with approximate attitude dynamics. Coupling between lateral-directional and longitudinal motion is ignored, as well as the coupling between speed and altitude.

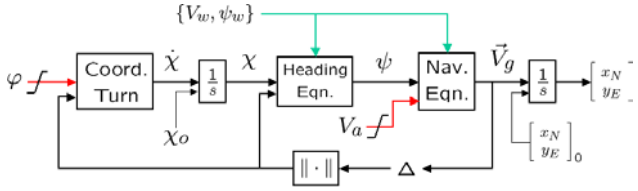

Fig. 7 The Planar-Kinematic model with control and disturbance inputs. Δ represents a delay. The *Coord. Turn* is Eqn(14), the *Heading Eqn.* is Eqn(15), and the *Nav. Eqn.* represents Eqns(1), (10), and (11).

For guidance algorithmic design, position and velocity information is assumed to be available at sufficient frequency. However, the quantization and processing delay of position and velocity feedback signals is included as:

$$\widehat{\vec{p}} = \vec{p}(\lfloor t/\Delta_k \rfloor \Delta_k - \Delta) \quad (18)$$
$$\widehat{\chi} = \chi(\lfloor t/\Delta_k \rfloor \Delta_k - \Delta) \quad (19)$$

where Δ_k is the sampling time, and Δ a pure delay, $\lfloor x \rfloor$ is the largest integer $\leq x$. For example, pure GPS data is typically available at $\Delta_k \approx 1s$.

5. CONSIDERATIONS FOR DESIGN OF GUIDANCE ALGORITHMS

5.1. Course-rate-of-change versus yaw-rate

In design of the guidance laws for inertial orbiting in strong winds, a distinction must be made between the inertial course rate-of-change and the heading rate-of-change. This is not commonly addressed in the literature. To visualize the effect of wind on the course-rate-of-change as compared with yaw-rate, we manipulate expressions (2) and (3) to obtain:

$$V_g^2 = V_a^2 + V_w^2 - 2V_a V_w \cos(\psi - \psi_w) \quad (20)$$
$$\tan\chi = \frac{V_a \sin\psi - V_w \sin\psi_w}{V_a \cos\psi - V_w \cos\psi_w} \quad (21)$$

Consider that V_w, and ψ_w are constant, and V_a varies slowly. Suppose for convenience that $\psi_w \equiv 90^o$, then we can find from Eqn(21) that:

$$\frac{\dot{\chi}}{\dot{\psi}} = \frac{\cos^2\chi}{\cos^2\psi} \left\{ 1 - \left(\frac{V_w}{V_a} \right) \sin\psi \right\} \quad (22)$$

Combining this expression with Eqn (21) we can express how the yaw-rate compares to the course-rate-of-change in various orientations and for various wind speeds. The result is shown in figure 8, which shows that the course-rate-of-change can be dramatically different from the yaw-rate in strong winds, e.g. the course-rate-of-change is up to 70% faster than the yaw-rate when $V_w = 10m/s$ while flying at $V_a = 25m/s$.

If we allow for arbitrary wind-direction, Eqn(22) becomes:

$$\frac{\dot{\chi}}{\dot{\psi}} = \frac{\cos^2\chi}{(\cos\psi - V_w/V_a \cos\psi_w)^2} \left\{ 1 - \left(\frac{V_w}{V_a} \right) \cos(\psi - \psi_w) \right\}$$

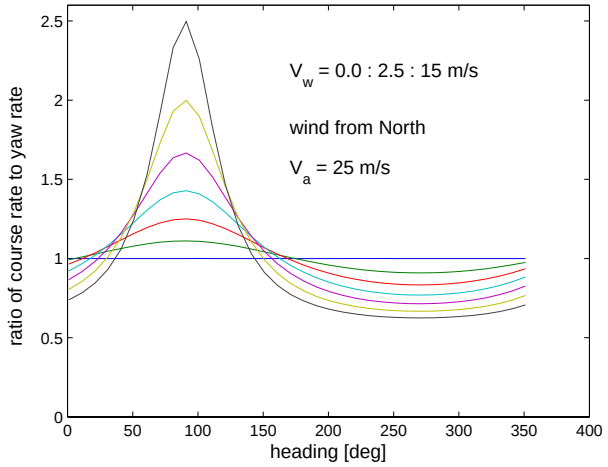

Fig. 8 Course-rate-of-change to yaw-rate ratio in various wind speeds while vehicle has an airspeed of $25\ m/s$**.**

5.2. The coupling of inertial speed and bank angle

The coupling of the bank-angle dynamics and nonlinearities (bank-angle and roll-rate saturation) with tight radius path following dynamics is exacerbated by the effect of wind. The effect of inertial speed on kinematics will form an important disturbance on path following performance. It is therefore of interest to see the explicit effects of inertial speed and orbit radius on the guidance laws.

From Eqns(14) and (16), the aircraft course rate of change about straight and level flight behaves approximately as:

$$\tau_\phi \Delta\ddot{\chi} \;=\; -\Delta\dot{\chi} + \frac{g}{V_g}\Delta\phi_c \tag{23}$$

where for this aircraft $\tau_\phi \approx 1/2.7\ s$. The kinematics of a constant altitude steady state turn may be approximated as (assuming coordinated turn with negligible pitch angle):

$$\phi_c \;=\; \arctan\left(\frac{V_g}{g}\dot{\chi}\right) \tag{24}$$

or, expressed in orbit radius:

$$\phi_c \;=\; \arctan\frac{V_g^2}{gR} \tag{25}$$

When linearized about a straight course, i.e.:

$$\begin{aligned}\phi_c &= \phi_{c\,o} + \Delta\phi \\ \dot{\chi} &= \dot{\chi}_o + \Delta\dot{\chi}\end{aligned}$$

where $\phi_{c\,o} = \dot{\chi}_o = 0$, Eqn(24) is approximately

$$\Delta\phi_c \approx \frac{V_g}{g}\Delta\dot{\chi} \tag{26}$$

This is the steady state of the roll bank angle to course dynamics in Eqn(23). When linearizing Eqn(24) about a nonzero steady state bank angle, as is the case in orbiting, we obtain:

$$\Delta\phi_c(\Delta\dot{\chi}) \;\approx\; \left\{1 + \left(\frac{V_g}{g}\dot{\chi}_o\right)^2\right\}^{-1}\frac{V_g}{g}\Delta\dot{\chi} \tag{27}$$

If the aircraft operates at some nominal inertial speed V_o, and considering that

$$V_o \;\equiv\; R_o\dot{\chi}_o \tag{28}$$

Then the change from the nominal bank angle due to changes in inertial speed can be approximated as:

$$\Delta\phi_c(\Delta V_g) \;\approx\; \left\{1 + \left(\frac{V_o^2}{g\,R_o}\right)^2\right\}^{-1}\left(\frac{2V_o}{g\,R_o}\right)\Delta V_g \tag{29}$$

ulation and the effect of wind.

5.3. The coupling of radius and bank angle

When Eqn(25) is linearized about an arbitrary nominal orbit, with

$$\Delta R \triangleq R - R_o \tag{30}$$

we have approximately

$$\Delta\phi_c(\Delta R) \;\approx\; -\left\{1 + \left(\frac{V_g^2}{g\,R_o}\right)^2\right\}^{-1}\left(\frac{V_g^2}{g\,R_o}\right)\frac{\Delta R}{R_o} \tag{31}$$

Eqns(29) and (31) may be useful to indicate potential bank angle limit encounters, and when inverted can be used to prevent integrator wind-up in the guidance algorithms due to bank-angle and roll-rate limits.

6. DESIGN OF THE GUIDANCE ALGORITHMS

Proportional closed loop airspeed manipulation

The open loop effect of airspeed manipulation on the phasing is a direct combination of Eqns(8), and (1). To manipulate the relative phase angle with control of inertial speed, a simple proportional feedback from phase angle to inertial speed can be constructed based on Eqn(8), see figure 9. If we select the gain from phase angle error to commanded inertial speed as

$$K \;=\; k\,R_o \tag{32}$$

then we can design the settling time entirely with k, since the (idealized, i.e. inerital speed can be directly manipulated, and no limitation on speed) closed loop would behave as:

$$\Delta\psi_p \;=\; \frac{K}{s\,R_o + K}\,\Delta\psi_c \tag{33}$$

$$\;=\; \frac{k}{s+k}\,\Delta\psi_c \tag{34}$$

where k would be selected for desirable settling time while avoiding coupling with engine dynamics.

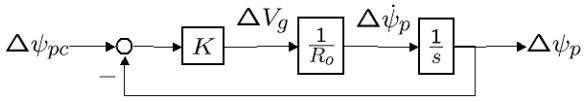

Fig. 9 Effect of ground speed on proportional phase angle control loop.

The fact that we manipulate airspeed, and that it is limited to e.g. $20 < V_a < 30[m/s]$, will have an effect on the closed loop as proposed. A linear approximation of the relation between inertial speed and airspeed as a function of clock angle can be obtained from Eqn(5), which was derived for $\psi_w \equiv 0$. For each vehicle this approximation is:

$$\Delta V_g \;\approx\; \left\{1 - \left(\frac{V_w}{V_{a\,o}}\right)\cos^2(\psi_p)\right\}^{-1/2}\Delta V_a \tag{35}$$

$$\;\approx\; \left\{1 + \left(\frac{V_w}{V_{a\,o}}\right)\frac{\cos^2(\psi_p)}{2}\right\}\Delta V_a \tag{36}$$

We can use this expression to investigate the effect of the ratio $V_w/V_{a\,o}$ on the performance of the control law.

Results of controlling the relative phase angle to 90^o in North wind of $10\ m/s$ by varying airspeed of both vehicles within the range $20 < V_a < 30[m/s]$ is shown below in figures (19) through (22). These results are compared with a combination of airspeed and radius manipulation. The radius manipulation is explained next.

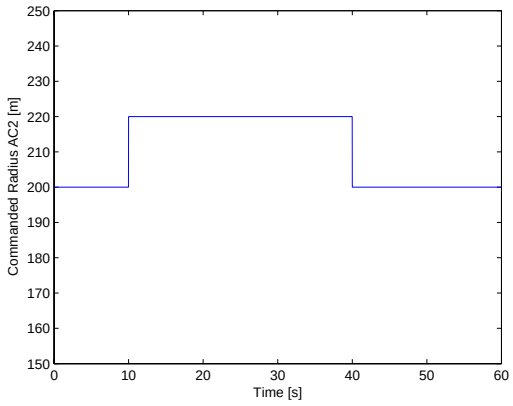

Fig. 10 Open loop commanded change in radius for vehicle #2.

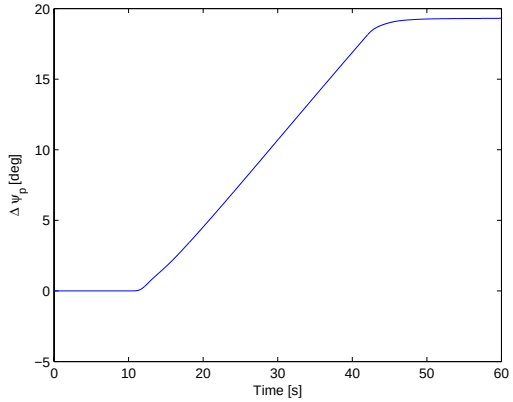

Fig. 11 Open loop change in relative phase angle as a result of commanded change in radius.

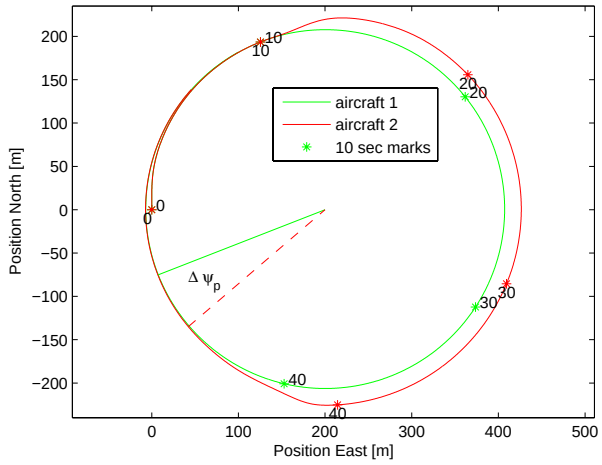

Fig. 12 Open loop orbits and positions for vehicles #1 and #2.

Open loop radius change

Figures 10, 11, and 12 show that it should be possible to use manipulation of the radius to separate the vehicles, and possibly to maintain that separation in wind conditions. To maintain the target-image calibration between the two vehicles, the orbits can not differ dramatically. If one of the vehicles looses track of the target, re-coordination must be established by co-locating the vehicles in orbit.

Proportional closed loop

A possible phase-angle tracker may be designed by feeding back the relative phase angle to a commanded change in radius. To limit the change in radius to reasonable values, a nonlinear feedback is necessary, e.g. by limiting the radius change to ±25%. Figures 13, 14, and 15 show how direct feedback from phase angle error to commanded radius yields the desired result, but that the desired phase angle difference is approached asymptotically. Hence, a nonlinear feedback is preferable.

Nonlinear closed loop

A nonlinear feedback of phase angle error to the commanded radius for vehicle #2 can improve the response of the relative phase angle to resemble that of the open loop response in figure 11. The results of using a sigmoidal or 'soft-step' type function in the feedback of relative phase error to commanded radius for vehicle #2,where the radius is limited to ±10% of the nominal, are shown in figures 16, 17, and 18. The result in figure 17 is close to the maximum performance to be expected given the design of the path following algorithm. However, figure 18 reveals a problem that appears to include coupling of the convergence to path, the radius of that path, the bank angle dynamics, aggravated by the nonlinear feedback loop.

7. RESULTS

A comparison of the guidance loops to maintain a relative phasing of 90^o is shown in figures (19) through (22). This describes the following scenario:

Commanded phasing	$\Delta\psi_{pC} = 90^o$
Wind	10 m/s from North
Nominal airspeed	$V_{a1} = V_{a2} = 25\ m/s$
Range of airspeed	$20 \leq V_a \leq 30\ m/s$
Nominal radius	$R_1 = R_2 = 200\ m$
Range of radius	$180 \leq R_2 \leq 220\ m$
Initial position	vehicles co-located West of tgt.
Initial heading	both vehicles heading North

Figure (19) compares the relative phasing for the above situation with manipulation of airspeed and both with, and without manipulation of radius. The vehicles start out co-located. In about twenty seconds they are phased at 90^o. Perturbations on phasing occur when airspeed limits are reached, as indicated in figure (20). The cause of these perturbations is reflected in figure (21), which show traces of the ground speed of both vehicles. When airspeed limits are reached, the ground speeds of the two vehicles differ. If no airspeed limits are reached the upper traces would be identical. The bottom traces include manipulation of the radius for vehicle 2, and therefore the ground speed will show subtle differences even when airspeed limits are not reached.

Figure (22) displays the radii for both situations for both vehicles. The upper traces are merely the perturbations of the nominal of the commanded $R_o = 200m$. The bottom traces include the manipulation of commanded R_2.

Figure (23) shows the corresponding planar inertial accelerations of the vehicles for the constant radius case. The acceleration traces for the case where R_2 is manipulated are similar. This figure is of interest to see at what clockangle the maximum acceleration and deceleration is

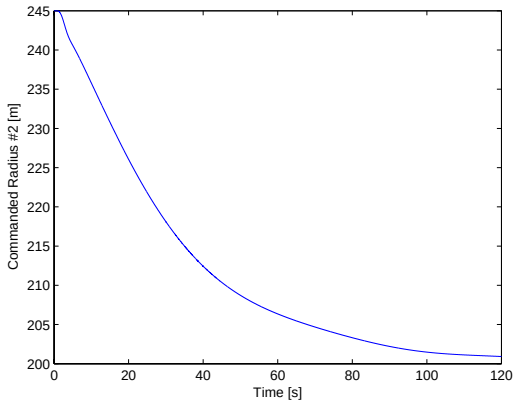

Fig. 13 Closed loop commanded change in radius for vehicle #2.

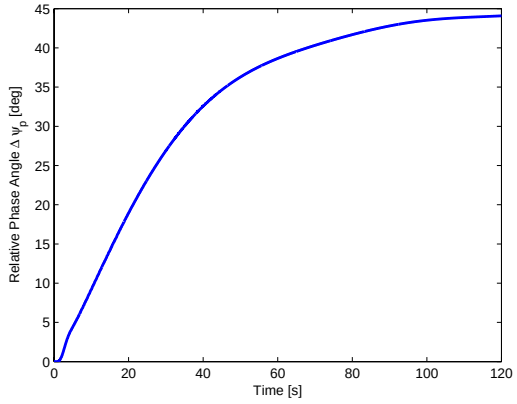

Fig. 14 Change in relative phase angle as a result of simple proportional feedback from phase angle error to radius.

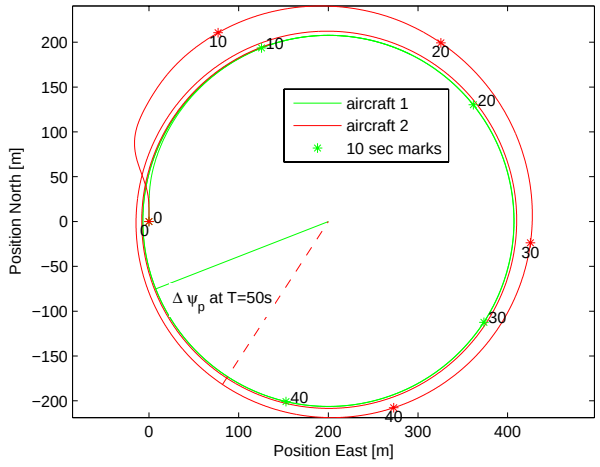

Fig. 15 Corresponding orbits and positions for vehicles #1 and #2, as a result of simple proportional feedback from phase angle error to radius. The desired phase angle difference is approached asymptotically.

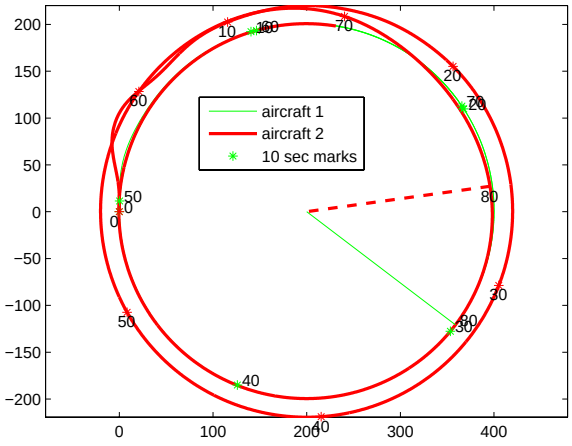

Fig. 16 Orbits and positions for vehicles #1 and #2, as a result of nonlinear feedback from phase angle error to radius. The desired phase angle difference is approached in finite time.

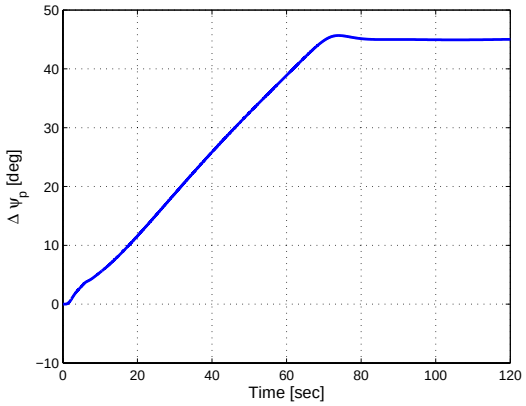

Fig. 17 Change in relative phase angle as a result of nonlinear feedback from phase angle error to radius.

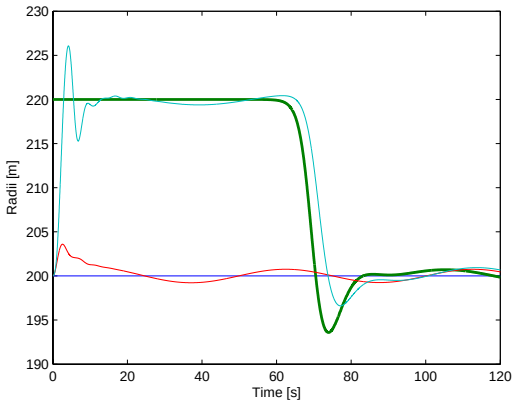

Fig. 18 Closed loop commanded radii, with the change in radius for vehicle #2. Also shown are traces of the actually flown radii. (Overshoot is due to integrator wind-up.)

engine-propeller dynamics (currently modeled to allow accelerations of approximately three g's).

8. IMPLEMENTATION OF PATH FOLLOWING

It is assumed that desired strategic paths have been generated and communicated to the individual vehicles, e.g. by the ECoPS path-planner.[4]

The Payload takes input from the INS (IMU/GPS) and contains a coordinate transformation that converts inertial position and velocity information to position and velocity relative to the desired path.

The purpose of the coordinate transformation is twofold; to conveniently express deviation from the path, and to measure progress along the path. The first is used for convergence strategy by the Helmsman. The second as a measure of progress along the path, independent of whether the vehicle has converged with it.

In the following, (see Fig 24)

$$
\begin{aligned}
y_s &= \text{the cross track error measured from the vehicle to the c} \\
s &= \text{arclength position along desired path} \\
\rho(s) &= \text{radius of the path at point } s \\
\kappa(s) &= \text{curvature of path } \triangleq 1/\rho(s) \\
\chi_s(s) &= \text{direction (from North) of path at point } s
\end{aligned}
$$

Frame $\mathcal{F}_s$ moves with the vehicle on the desired path, with $\mathbf{x}_s$ in the direction of the desired inertial velocity, i.e tangential to the path, and $\mathbf{y}_s$ normal to the path. Assume coordinated level flight; $u_b \approx V_g$ and $v_b = 0$. The *relative course* is defined as

$$\widetilde{\chi} \triangleq \chi - \chi_s \tag{37}$$

The actions of the Payload processor are represented in figure 25. The individual $\mathcal{F}_s$ path variables are related to aircraft states by the following expression, represented by the matrix in figure 25:

$$\dot{y}_s = \sin(\widetilde{\chi})\, V_g \tag{38}$$

$$\dot{s} = \frac{\cos(\widetilde{\chi})}{1 - \kappa\, y_s} V_g \tag{39}$$

$$\dot{\chi}_s = \kappa \dot{s} \tag{40}$$

$$\dot{\widetilde{\chi}} = \dot{\chi} - \dot{\chi}_s \tag{41}$$

Limitation: Eqn(39) and (41) are not usable when $y_s = \frac{1}{\kappa(s)} = \rho(s)$, i.e. when the vehicle is at the center of the instantaneous circle.

9. CONSTRUCTION OF SIGNALS FOR THE HELMSMAN STRATEGY

In the following, a turn-rate command (or an equivalent bank-angle command) is constructed based on the helmsman behavior with the goal to follow the desired path. It is assumed that the wind $\{V_w, \psi_w\}$ are known (estimated), the airspeed V_a and altitude remain approximately constant, bank angle command following performs well and fast relative to path-changes of $\pm 30^o$, and the commanded path will be mild enough to prevent extreme wind-up of path-following integral action due to roll-rate and saturation limits. The latter is a temporary assumption, hedging of the commanded heading rate will be implemented later.[5]

The input to the helmsman is the cross track error y_s, the relative course $\widetilde{\chi}$, and the ground speed V_g. The output is a turn rate command, which can be translated kinematically into a bank angle command.

Let the ideal course convergence dynamics be specified as follows

$$\frac{d}{dt}\chi(t) = \dot{\chi}_{com} \tag{42}$$

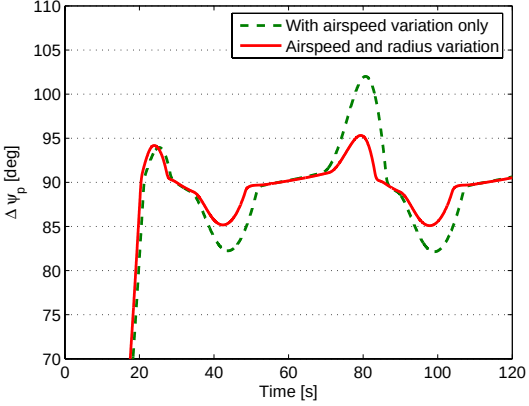

Fig. 19 Relative phasing for case of airspeed manipulation with and without manipulation of radius of vehicle 2.

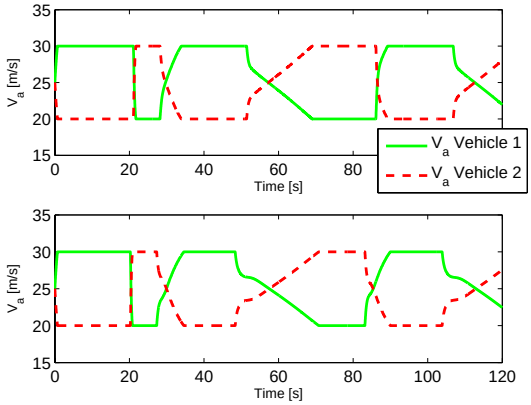

Fig. 20 Airspeeds with and without manipulation of radius of vehicle 2.

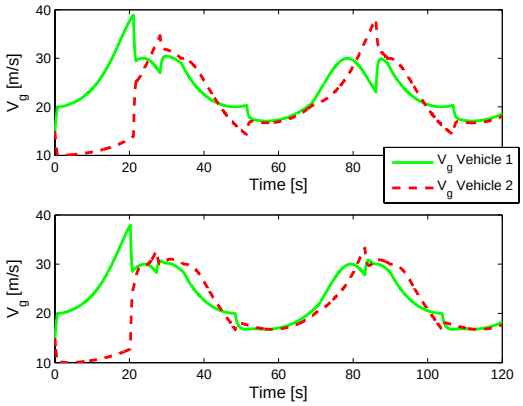

Fig. 21 Ground speeds with and without manipulation of radius of vehicle 2.

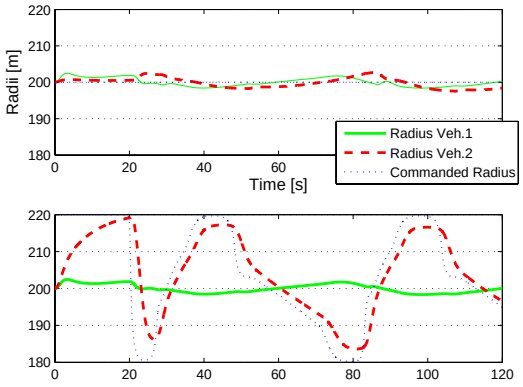

Fig. 22 Actual radii with and without manipulation of radius of vehicle 2.

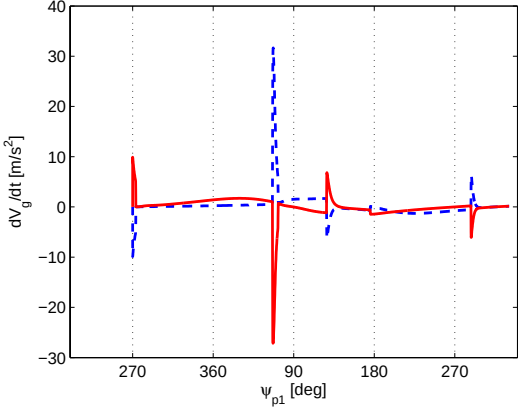

Fig. 23 Inertial accelerations of both vehicles with airspeed manipulation.

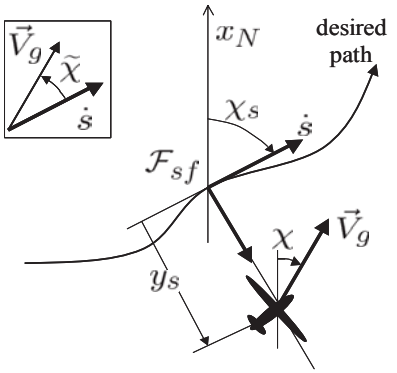

Fig. 24 The 'Serret-Frenet' coordinate transformation for a 2D-path. The Serret-Frenet frame provides a means to ride along the 2D curve and illustrate its properties (curvature).

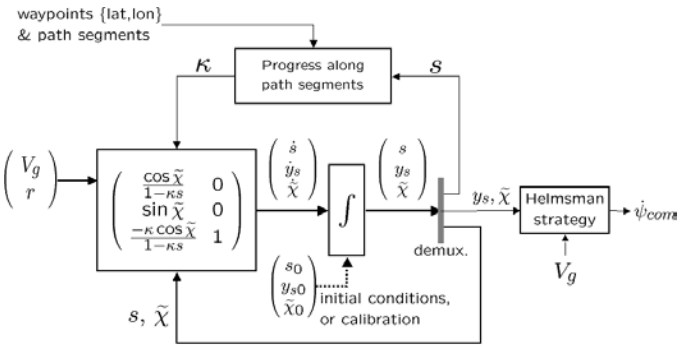

Fig. 25 The coordinate transformation part of the *Payload Processor*, where V_g is the inertial speed, $r \approx \dot{\chi}$ the yaw rate, and the path segments are received from the path planner / trajectory generator.

where $\dot{\chi}_{com}$ is a control law

$$\frac{d}{dt}\chi_{com}(t) \; = \nu(\chi, \chi_c) \tag{43}$$

where, to avoid adding integrator dynamics and its associated implementation woes, we used a simple proportional design with a feedforward term:

$$\nu \;\; = \;\; k_p'(\widetilde{\chi}_c - \widetilde{\chi}) + \kappa V_g \tag{44}$$

where κV_g is a kinematics feedforward term that replaces the need for integral action for constant curvature path following. Herein $\widetilde{\chi}_c$ denotes the commanded intercept course based on the helmsman behavior, defined by

$$\sigma(y_s) \;\triangleq\; \widetilde{\chi}_{icpt}\frac{e^{-2a\,y_s}-1}{e^{-2a\,y_s}+1} \tag{45}$$

In a coordinated turn, the bank angle is kinematically related to the turn rate as

$$\tan(\phi) \; = \frac{V_g}{g}\dot{\psi} \tag{46}$$

with the approximation

$$\dot{\psi} \approx \dot{\chi} \tag{47}$$

This approximation does not necessarily hold when orbiting in strong wind, as indicated in Figure 8. The effect of this remain to be addressed. The commanded turn rate is mapped to a commanded bank angle as

$$\phi_c \; = \arctan(\frac{V_g}{g}\,\nu) \tag{48}$$

10. SUMMARY HELMSMAN STRATEGY IMPLEMENTATION

The sequence of computations for the helmsman can be summarized as in Figure 26 with

1. The sigmoidal function

$$\sigma(y_s) \;\; = \;\; \widetilde{\chi}_{icpt}\frac{e^{-2a\,y_s}-1}{e^{-2a\,y_s}+1} \tag{49}$$

2. A pseudo-control signal, representing the desired yaw rate, can be determined with input variables $(y_s, V_g, \widetilde{\chi})$ and parameter κ as

$$\dot{\chi}_{com} \;\; = \;\; V_g\kappa + k_p\,[\sigma(y_s) - \widetilde{\chi}] \tag{50}$$

3. If necessary, the above strategy can be achieved by means of a bank-angle command, as determined by the approximate expression

$$\phi_c \; = \arctan(\frac{V_g}{g}\,\nu) \tag{51}$$

4. These expressions still need to be enhanced with the effects of

$$\frac{\dot{\chi}}{\dot{\psi}} \;\; = \;\; \frac{\cos^2\chi}{\cos^2\psi}\left\{1 - \left(\frac{V_w}{V_a}\right)\sin\psi\right\} \tag{52}$$

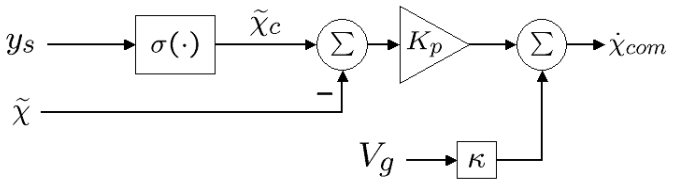

Fig. 26 The helmsman reference model, representing the behavior of a 'good helmsman'. Its output is a desired turn rate signal. (Note that the difference in $\dot{\psi}_{com}$ and $\dot{\chi}_{com}$ needs to be addressed according to Eqn.??, this remains to be investigated further.) The desired relative course is a function of cross-track distance saturating at an intercept angle ($< 90^o$, e.g. in commercial aviation this is typically 30^o). A similar strategy can be applied for altitude.

Asymmetry in Helmsman Dynamics

The helmsman produces a course-rate-of-change command based on lateral deviation from the desired track.[3] When the aircraft is already banked in a nominal radius orbit, the convergence with a larger radius orbit will differ from that with a tighter orbit (due to both geometry and bank angle nonlinearities), figures 27 and 28. These

integrator windup protection with respect to the bank angle and roll-rate limits. However, this can be further addressed by adding some asymmetric helmsman compensation in the yaw-rate to commanded roll relation that aims for a more aggressive intercept angle when converging with a tighter orbit, and v.v. when needing to ease up and converge with a milder orbit. For example, when converging with a path from the inside of a curve, the intercept angle can be milder, say 30^o, when converging from the outside it will be more aggressive 45^o. This leads to quicker response, see Figures 29 and 30. The asymmetric sigmoidal nonlinearity for the helmsman in this example was defined as

$$\begin{aligned} s_\kappa &= |\kappa_o| \times sign\left(\kappa_o\, y_s\right) \\ \tilde{\chi}_{icpt} &= -7.5 * \kappa_o * s_\kappa + 37.5^o \\ \sigma(y_s) &= -\tilde{\chi}_{icpt} * \frac{e^{2a\, y_s} - 1}{e^{2a\, y_s} + 1} \\ \tilde{\chi}_c &= -\sigma(y_s) \end{aligned}$$

where in this example $\kappa_o = 1/200$, and where s_κ is a parameter proportional to κ_o that indicates whether the vehicle is converging from inside or outside the curve. This design will command a 45^o maximum intercept when converging from the outside, and a 30^o maximum coming from the inside. Although this asymmetric design is smooth, it is not a function of ground speed. Ground speed will be a major factor in the convergence dynamics, as well as in vehicle capabilities.

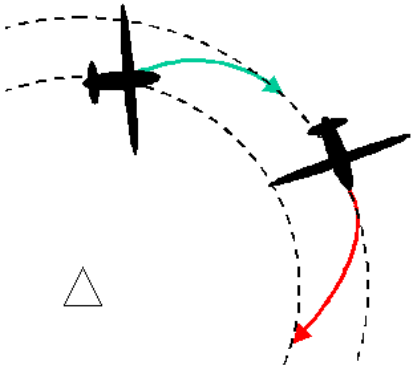

Fig. 27 Asymmetry in the convergence with orbital tracks.

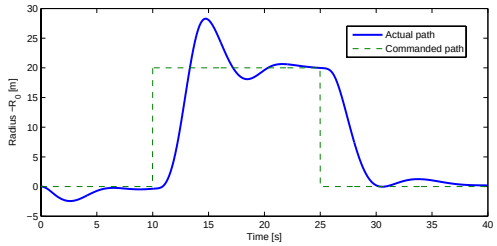

Fig. 28 Nonlinearity in the bank-angle to yaw-rate response. Note the difference in overshoot between going outward and coming back to the inner radius.

REFERENCES

[1]Ousingsawat, J. and Campbell, M., "Establishing Trajectories for Multi-Vehicle Reconnaissance," *AIAA 2004-5224*.

[2]"The Insitu Group," Seascan UAV Specifications, http://www.insitugroup.net/pages/Products/seascanSpecs.html.

[3]Rysdyk, R., "UAV Path Following for Constant Line-of-Sight," *AIAA 2003-6626*, San-Diego, CA.

[4]Pongppunwattana, A. and Rysdyk, R., "Real-Time Planning for Multiple Autonomous Vehicles in Dynamic Uncertain Environments," *AIAA JACIC*, December 2004, pp. 580–604.

[5]Johnson, E. N., *Limited Authority Adaptive Flight Control*, Ph.D. thesis, Georgia Institute of Technology, School of Aerospace Engineering, Atlanta, GA 30332, dec 2000.

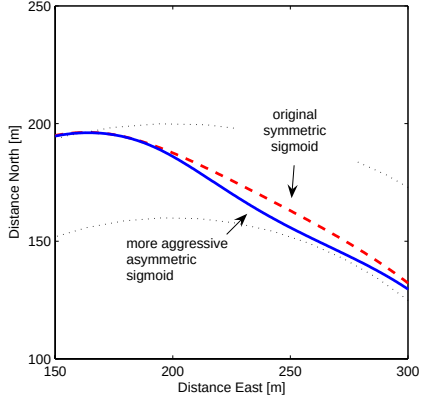

Fig. 29 Flight path corresponding to first orbit change in Figure 30, over time range $10 - 15[s]$ approximately.

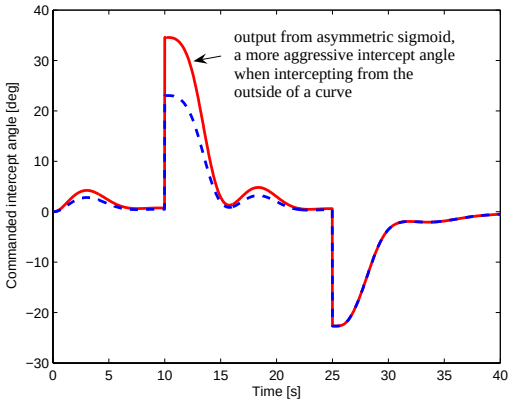

Fig. 30 Asymmetric intercept angles for path convergence from inside and outside of a curve.